JOURNAL OF Materials CHEMISTRY

Synthesis, structure and properties of a new two-photon photopolymerization initiator

Yan Ren,*[a] Xiao-Qiang Yu,[a] Dong-Ju Zhang,[b] Dong Wang,[a] Ming-Liang Zhang,[c] Gui-Bao Xu,[a] Xian Zhao,[a] Yu-Peng Tian,[c] Zong-Shu Shao[a] and Min-Hua Jiang[a]

[a]*State Key Laboratory of Crystal Materials, Shandong University, Jinan, 250100, P. R. China. E-mail: ry@icm.sdu.edu.cn*
[b]*School of Chemistry and Chemical Engineering, Shandong University, Jinan, 250100, P. R. China*
[c]*School of Chemistry and Chemical Engineering, Anhui University, Hefei, 230039, P. R. China*

Received 8th July 2002, Accepted 19th September 2002
First published as an Advance Article on the web 23rd October 2002

A new two-photon free-radical photopolymerization initiator, (*E*,*E*)-4-{2-[*p*′-(*N*,*N*-di-*n*-butylamino)stilben-*p*-yl]vinyl}pyridine (abbreviated to DBASVP), has been synthesized. Quantum chemistry calculations showed that the new initiator possesses a large delocalized π electron system, a large change in dipole moment on transition to the excited state and a large transition moment. The calculated two-photon absorption cross-section is as high as 881.34 × 10^{-50} cm^4 s $photon^{-1}$. The single-photon and two-photon absorption and fluorescence properties in various solvents have been investigated carefully. The new initiator exhibits outstanding solvent-sensitivity, which experimentally interprets the excellent electron delocalized properties of the molecule. A microstructure has been fabricated under irradiation at 800 nm using a 200 fs, 76 MHz Ti:sapphire femtosecond laser.

Introduction

In two-photon absorption (TPA), the excitation is confined to a small focal volume due to the quadratic dependence of absorption on the incident intensity. This characteristic of two-photon processes has made two-photon absorption based photopolymerization an effective tool for processing photonic devices, micromachines, zero-threshold lasers and integrated optical waveguides in three dimensions with high spatial resolution.[1–4]

For two-photon free radical photopolymerization, the polymerization rate and photoinitiation threshold is closely related to the absorption behavior of the initiator at the excitation wavelength (generally twice its single-photon absorption wavelength). At present, effective initiators are still rare because the design strategy, or in other words, the relationship of the initiator structures and their properties for initiating two-photon photopolymerization, remained unclear. Consequently, commercially available UV photopolymer initiators are often used as substitutes in two-photon 3D microfabrication. Unfortunately, these initiators always exhibit low photosensitivity due to their small two-photon absorption cross-section. Therefore, the search for effective and high photosensitive two-photon photopolymerization initiators is urgently required.

Some approaches to improving the photosensitivity of photoinitiator molecules that have been reported are based on the idea of increasing their two-photon absorption cross-sections.[5] According to Albota *et al.*[6] and Reinhardt *et al.*,[7] the conjugation length, donor and acceptor strength, and planarity of the π center are the important parameters for enhancing the TPA. On the basis of this design strategy, in this article, (*E*,*E*)-4-{2-[*p*′-(*N*,*N*-di-*n*-butylamino)stilben-*p*-yl]vinyl}pyridine (abbreviated to DBASVP), which possesses a large π conjugated system and a strong donor and acceptor group, has been synthesized using a relatively simple route. This compound exhibits a strong two-photon absorption at ~830 nm. A microstructure has been fabricated using this new initiator. It was proved be an effective two-photon photopolymerization initiator excited with an 800 nm, 200 fs, 76 MHz Ti:sapphire laser source. Because of its intriguing properties as a new near-IR two-photon free-radical photoinitiator, we have also conducted a thorough study of its structure by quantum chemistry calculations and investigated its spectroscopic properties including single-photon and two-photon fluorescence in different solvents in order to get an understanding of the structure–spectroscopy–property relationship and to promote the design of new effective two-photon photoinitiators.

Experimental

1 Chemicals

4-Vinylpyridine (95%), palladium(II) acetate (47.5% Pd) and 4-bromobenzyl bromide (98%) were products of Acros Organics. *N*,*N*-Di-*n*-butylaniline (>98%) and tris(2-methylphenyl)phosphine (>95%) were purchased from Tokyo Kasei Kogyo Co., Ltd. Triphenylphosphine was AR grade. The above chemicals were used without further purification. *N*,*N*-Dimethylformamide, phosphorus trichloride and triethylamine and all solvents were purified before use. A *tert*-butoxide–*tert*-butyl alcohol solution was prepared immediately before use.

Photoluminescence and absorption measurements were conducted in various solvents including toluene, chloroform, THF, diethyl ether, ethanol, methanol, benzyl alcohol, acetone, acetonitrile and *N*,*N*-dimethylformamide (DMF). All of the above solvents were anhydrous grade after further purification. Moreover, each of the solutions used for the single-photon fluorescence measurements was freshly prepared and kept in the dark before the measurements. The solution concentration was 1 × 10^{-5} mol L^{-1}.

2 Instruments

The 300 MHz ^{1}H NMR spectra were obtained on an INOVA-300 spectrometer. Elemental analysis was performed using a

PE 2400 elemental analyzer. The electrospray mass spectrum (ES-MS) was determined on a Finnigan LCQ mass spectrograph; the concentration of the sample was about 1.0 mmol L^{-1}. The diluted solution was electrosprayed at a flow rate of 5×10^{-6} L min^{-1} with a needle voltage of + 4.5 kV. The mobile phase was an aqueous solution of methanol (v/v, 1 : 1) acidified with acetic acid. The sample was run in the positive-ion mode.

UV-vis-near-IR spectra were measured on a Hitachi U-3500 recording spectrophotometer. The steady-state fluorescence spectra measurement was performed using an Edinburgh FLS920 spectrofluorimeter. A 450 W Xe arc lamp provides the ~400 nm excitation source. Spectra were recorded between 420 nm and 780 nm using a photomultiplier tube as detector, which is operated in the single photon counting mode. The spectral resolution is 0.1 nm. The quartz cuvettes used were of 1 cm path length.

3 Synthesis

The synthetic route is shown in Scheme 1.

4-(*N*,*N*-Di-*n*-butylamino)benzaldehyde (1). Dimethylformamide (100 mL) was cooled to 0 °C and treated dropwise with phosphorus oxychloride (21 mL, 225 mmol). The solution was stirred at 0 °C for 1 hour and at room temperature for another 1 hour. To the red solution was added dropwise *N*,*N*-di-*n*-butylaniline (45.3 mL, 200 mmol). The mixture was heated at 60 °C for 10 hours and then cooled to 0 °C. Then a solution of 20 g of sodium acetate in 200 mL of cold water was added slowly with stirring. The reaction mixture was then stirred for an additional hour and the resulting solution was extracted with diethyl ether. The combined extract was washed with saturated anhydrous sodium bicarbonate and then washed with water and the organic layer was dried over anhydrous magnesium sulfate. Then the solvent was removed under reduced pressure, and the residue was distilled in vacuum at ~148 °C, 1 mmHg. 24 g 4-(*N*,*N*-Di-*n*-butylamino)benzaldehyde was obtained as a yellow liquid.

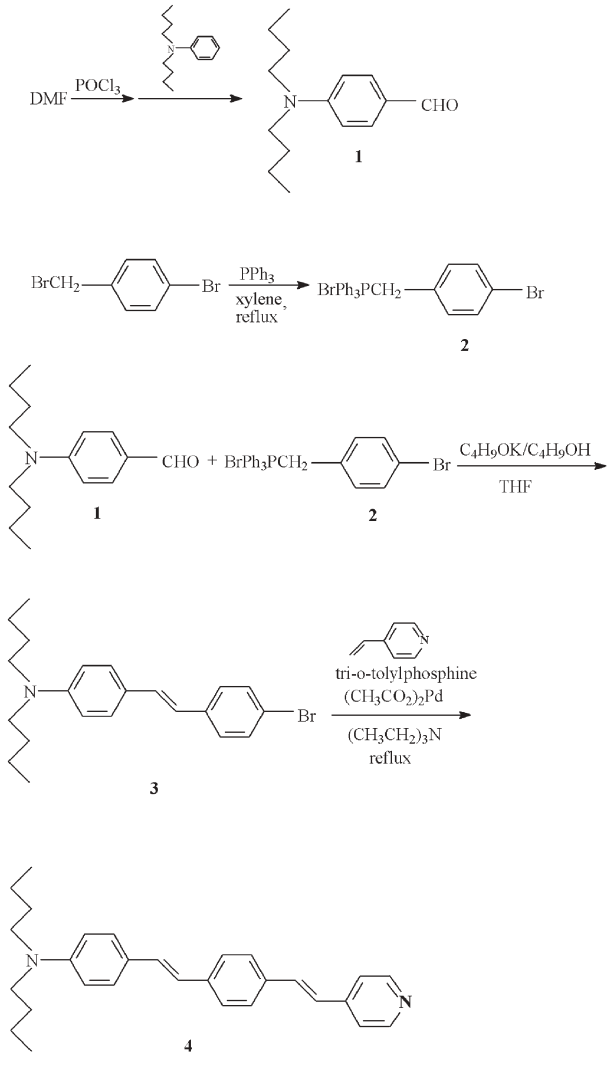

Scheme 1

4-Bromobenzyl(triphenyl)phosphonium bromide (2). To a 250 mL flask with a stirrer, 25 g (0.10 mol) 4-bromobenzyl bromide, 30 g (0.11 mol) triphenylphosphine and 200 mL xylene were added. The reaction mixture was refluxed for 6 hours, then cooled to room temperature and filtered. The resulting white solid was washed with diethyl ether three times and re-crystallized in a 3 : 1 mixture of chloroform and ethanol. 23 g colorless crystals were obtained. Yield: 45%.

4-Bromo-4′-(*N*,*N*-di-*n*-butylamino)stilbene (3). To a 250 mL four-necked flask with a magnetic stirrer, a dropping funnel, a nitrogen input tube and an adapter with a stopcock, 15.36 g (0.03 mol) 4-bromobenzyl(triphenyl)phosphonium bromide were added under a nitrogen atmosphere. Then 4.66 g (0.02 mol) 4-(*N*,*N*-di-*n*-butylamino)benzaldehyde–THF solution were injected into the flask through the stopcock of the adapter. The reaction mixture was cooled to 0 °C in an ice bath, 0.15 mol potassium *tert*-butoxide–*tert*-butyl alcohol solution was added to the dropping funnel and was dropped into the flask at 0 °C over one and a half hours. After the reaction mixture had been stirred for two hours at 0 °C, the ice bath was removed and the mixture stirred at room temperature overnight and then for another two hours at 60 °C in an oil bath. After being cooled to room temperature, the product was poured into 200 mL distilled water, neutralized with dilute hydrochloric acid, and extracted with dichloromethane. The organic layer obtained was dried over anhydrous magnesium sulfate. After filtration, the solvent was removed from the solution at reduced pressure and the residue dissolved in a minimum of DMF. The solution obtained was chromatographed over 200 g of silica gel. Elution with 1 : 5 diethyl ether–petroleum ether and then recrystallization three times in ethanol produced light green crystals. Calcd for $C_{22}H_{28}BrN_2$: C, 68.39; H, 7.25; N, 3.63. Found: C, 68.56; H, 7.77; N, 3.76%. ^{1}H NMR ($CDCl_3$) (300MHz; TMS) δ_H: 0.95 (3H, t, *J* 7.2 Hz), 1.35 (2H, m), 1.51 (2H, m), 3.28 (2H, t, *J* 7.56), 6.62 (2H, d, *J* 8.59 Hz), 6.69 (1H, d, *J* 16.15 Hz), 7.01 (1H, d, *J* 16.15 Hz), 7.32 (2H, d, *J* 8.59 Hz), 7.36 (2H, d, *J* 8.94 Hz), 7.42 (2H, d, *J* 8.59 Hz).

(*E*,*E*)-4-{2-[*p*′-(*N*,*N*-Di-*n*-butylamino)stilben-*p*-yl)vinyl]pyridine (4). 1.5 g (3.75 mmol) 4-Bromo-4′-(*N*,*N*-di-*n*-butylamino)-stilbene, 0.49 g (1.61 mmol) tri-*o*-tolylphosphine, 0.87 mL (8.06 mmol) vinylpyridine, 0.045 g palladium(II) acetate (0.2 mmol) and 80 mL redistilled triethylamine under nitrogen, were added to a three-necked flask equipped with a magnetic stirrer, a reflux condenser, and a nitrogen input tube. The reaction mixture was refluxed in an oil bath under nitrogen. An orange product was obtained after heating and stirring for 16 h. Then the solvent was removed under reduced pressure and the residue was dissolved in methylene chloride, washed three times with distilled water, and dried with anhydrous magnesium sulfate. Then it was filtered and concentrated. The resulting solution was chromatographed over 200 g of silica gel. Elution with 3 : 2 ethyl acetate–petroleum ether and then recrystallization twice from diethyl ether produced light yellow crystals. ES-MS, *m*/*z* (%): 411.4 ($[M+H]^+$, 100), 206.2 (33). Calcd for $C_{29}H_{34}N_2$: C, 84.87; H, 8.29; N, 6.83. Found: C, 84.40; H, 8.74; N, 7.60%.

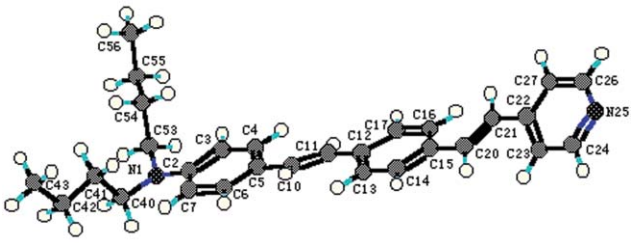

Fig. 1 Equilibrium geometry of DBASVP in a vacuum.

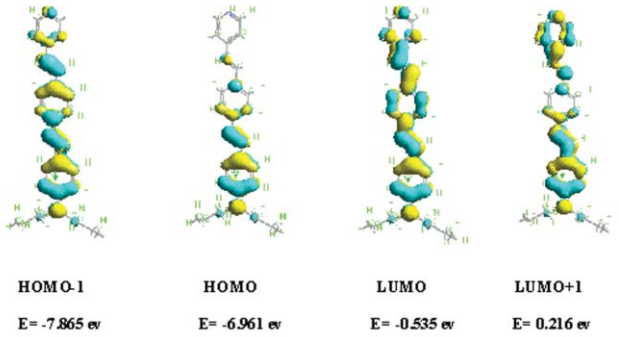

Fig. 2 Orbital energy and electron density distribution of frontier molecular orbitals.

4 Computation

The restricted Hartree–Fock (RHF) theory and quantum chemical parametrization AM1 (a modified neglect of differential overlap) in the program package MOPAC 6.0 were employed in the structural optimization.[8,9] Minimum-energy geometry was used for ZINDO CI calculations using the CNDO/1 method with the highest 15 occupied orbitals and the lowest 15 unoccupied (virtual) orbitals to determine the distribution of the frontier molecular orbitals, the corresponding electronic spectrum,[10,11] the state dipole and transition dipole moments, and oscillator strength. All parameters used in our calculations were the default values in the programs. The state dipole moment and transition moment were directly used to evaluate the two-photon absorption cross-section based on the two-state model. All computations were accomplished on an O2 workstation.

Results and discussion

1 Structural features

Fig. 1 depicts the equilibrium geometry of this compound in a vacuum. Table 1 lists the selected bond lengths, bond angles and dihedral angles. From Fig. 1, one can see that the molecule is not perfectly planar. According to Table 1, the dihedral angle of C11–C10–C5–C4, C12–C11–C10–C5 and C13–C12–C11–C10 are −15.9°, 179.8° and 15.9° respectively. Therefore, the two benzene rings are actually in same plane. The dihedral angles of C21–C20–C15–C14, C22–C21–C20–C15 and C23–C22–C21–C20 are −160.0°, −179.5° and 14.9° respectively. The angle between the pyridine ring and the benzene ring is ~34.4°. The bond lengths of the two benzene rings and the pyridinium ring are characteristic of aromatic bonds. The bridge bond lengths of C5C10, C10C11, C11C12 and C15C20, C20C21, C21C22 indicate that the bridge bonds are also highly conjugated.

The excited state calculation (ZINDO CI) was performed based on the *trans* orientation of the compound. The results show that transition between the ground state S_0 and the first excited state S_1 is mainly attributed to the promotion of an electron from the HOMO to the LUMO. The transition energy is 28489.1 cm^{-1} with the an oscillator strength (f) of 2.081. Fig. 2 illustrates the electron density distribution of the frontier molecular orbitals. In the HOMO, the electrons are mainly concentrated on the nitrogen atom of the amino and its adjacent benzene ring. While in the LUMO, the electrons are spread over the molecule along the molecular axis. Obviously, the electron density is shifted from the *N*,*N*-di-*n*-butylamino to the vinylpyridine upon excitation. The calculation results also show that this transition causes a large change in the molecular dipole moment ($\Delta\mu_{total}^{ge}$ = 6.600 D) and a large transition moment (M_{total}^{ge} = 12.454 D). The conjugated geometric configuration and the electron density distribution of the frontier molecular orbitals reveal that the molecule has a highly delocalized π-electron system. We consider that these structural features are necessary conditions for two-photon absorption and for initiating a photopolymerization reaction.

The two-photon absorption cross-section was evaluated based on the two-state model.[12,13] Generally, from the sum-over-state formulae, the two-photon matrix elements for the resonant absorption of two-photons with identical energy are expressed as

$$S_{\alpha\beta} = \sum_{i} \left[\frac{\langle o|\mu^{\alpha}|i\rangle\langle i|\mu^{\beta}|f\rangle}{\omega_i - \omega_f/2} + \frac{\langle o|\mu^{\beta}|i\rangle\langle i|\mu^{\alpha}|f\rangle}{\omega_i - \omega_f/2} \right] \quad (1)$$

where ω_f denotes the excitation energy of the excited state $|f\rangle$, μ is the electronic dipole operator, α and β denote the different orientation of x, y and z, o, i and f represent the ground, intermediate and final state, respectively; ω_i is the excitation energy for the intermediate state. For molecules in the gas phase and in solution, the TPA cross-section is given by

Table 1 The selected bond lengths (Å), bond angles (°) and dihedral angles (°) optimized by AM1

N1–C2	1.405	C11–C12	1.451	C20–C21	1.344
C2–C3	1.418	C12–C13	1.403	C22–C23	1.404
C3–C4	1.387	C13–C14	1.390	C23–C24	1.406
C4–C5	1.401	C14–C15	1.404	C24–N25	1.346
C5–C6	1.404	C15–C16	1.403	N25–C26	1.348
C5–C10	1.450	C17–C12	1.405	C27–C22	1.406
C10–C11	1.344	C20–C15	1.452		
N1–C2–C3	121.01	C12–C11–C10	124.88	C22–C21–C20	124.88
C2–C3–C4	121.19	C14–C13–C12	120.82	C23–C22–C21	122.97
C3–C4–C5	121.40	C15–C14–C13	120.79	C24–C23–C22	118.91
C4–C5–C6	117.81	C16–C15–C14	118.47	N25–C24–C23	123.76
C7–C2–C1	121.84	C17–C12–C11	119.14	C26–N25–C24	117.00
C10–C5–C4	123.00	C20–C15–C14	119.15	C27–C22–C21	119.38
C11–C10–C5	125.02	C21–C20–C15	124.55		
C11–C10–C5–C4	−15.92	C12–C11–C10–C5	179.83	C23–C21–C20–C15	−179.50
C13–C12–C11–C10	15.85	C21–C20–C15–C14	−160.02	C23–C22–C21–C20	14.92

orientational averaging over the two-photon absorption probability

$$\delta_{\mathrm{TPA}} = \sum_i \left[F S_{\alpha\alpha} S^*_{\beta\beta} + G S_{\alpha\beta} S^*_{\alpha\beta} + H S_{\alpha\beta} S^*_{\beta\alpha} \right] \quad (2)$$

where the coefficients F, H and G are related to the polarization of the radiation source. The values of F, H and G are 2, 2 and 2 for linear polarized light and -2, 3 and 3 for the circular one. For one dimensional molecules, however, some simplifications can be made according to the two-state model in which only the ground and first low-lying charge transfer excited state are taken into account and the TPA cross-section is believed to be completely dominated by the component along the z molecular axis, S_{zz},

$$S_{zz} = \frac{2\Delta\mu_z^{\mathrm{ge}} M_z^{\mathrm{ge}}}{\Delta E} \quad (3)$$

where $\Delta\mu_z{}^{\mathrm{ge}}$ and $M_z{}^{\mathrm{ge}}$ are the change in dipole moment and the transition moment respectively between the ground state and the first excited state, and $\Delta E = \hat{\imath}\omega$, where ω is the fundamental frequency of the light. Thus the TPA cross-section is given by

$$\delta_{\mathrm{TPA}} = \sum_{zz} \left[F S_{zz} S^*_{zz} + G S_{zz} S^*_{zz} + H S_{zz} S^*_{zz} \right] \quad (4)$$

The TPA cross-section directly comparable with experiment is defined as

$$\sigma_{\mathrm{TPA}} = \frac{4\pi^3 a_0^5 \alpha \omega^2}{15c} \frac{}{\Gamma_{\mathrm{f}}} \delta_{\mathrm{TPA}} \quad (5)$$

Based on the above model, the two-photon absorption cross-section σ_{TPA} of DBASVP was calculated. The state dipole and transition dipole moments obtained from ZINDO were directly used during the calculations. Assuming linear polarized light was used, the value calculated is as high as 881.34×10^{-50} cm^4 s photon^{-1}, which indicates that a strong two-photon absorption occurs upon excitation.

2 Linear absorption

According to the above quantum chemistry calculation results, the single-photon absorption peak in a vacuum is at 351 nm (28489.1 cm^{-1}, the oscillator strength $f = 2.081$). In fact, the single-photon absorption peak in solution was observed to deviate from that in a vacuum. Fig. 3 shows the resulting spectra observed experimentally. The absorption peak appears at 402 nm in cyclohexane (with the corresponding molar absorption coefficient $\varepsilon_{\max} = 27288$), 408 nm in toluene ($\varepsilon_{\max} = 36707$), 411 nm in chloroform ($\varepsilon_{\max} = 44052$), 422 nm in benzyl alcohol ($\varepsilon_{\max} = 40485$), 406 nm in acetone ($\varepsilon_{\max} = 48206$), 408 nm in ethanol ($\varepsilon_{\max} = 53364$), 405 nm in acetonitrile ($\varepsilon_{\max} = 48431$) and 411 nm in DMF ($\varepsilon_{\max} = 49947$) respectively. Above 525 nm, the solutions are completely transparent. The absorption deviation in solution can be attributed to the interaction of the solute with the local molecular environment including solvent molecules and other surrounding solute molecules. One can see that the peak position and peak broadening are different for different solutions, which further identify the effect of solvent on absorption behavior.

Some interesting results can be observed from Fig. 3. A slight red shift in absorption is observed in low polar solvents, while the absorption peaks are found to be blue shifted in high polar solvents such as acetone, ethanol, and acetonitrile. In order to avoid any possible error, the solutions were freshly prepared and the spectra measured again, but the same curves were obtained. The slight red shift in low polar solvents can be explained by the fact that the energy level of the excited state is reduced more than that of the ground state by solvent action since a relatively high polarity of DBASVP predominates in the excited state and a lower polarity predominates in the ground state (the values of μ_{g}, μ_{e}, are 5.604 D and 12.204 D respectively). When a D–A structural molecule is in a high polar solvent, the molecule in the ground state tends to be polarized to form a charge-separated molecule by the action of an electric field formed by the surrounding solvent molecules. We consider that the absorption blue shift of DBASVP in such a polar environment is like the blue shift behavior of zwitterionic hemicyanine dyes and pyridinium dyes. Compared to DBASVP,[14,15] generally, they show a large negative solvatochromism because of an opposite polar form in the ground and excited states. The corresponding quantum chemistry calculation is in progress in order to obtain a reasonable explanation for the solvatochromism of DBASVP.

3 Single-photon fluorescence

Steady state fluorescence. The single-photon fluorescence spectra of DBASVP show sensitivity to the polarity of the environment around DBASVP (see Fig. 4). There is a remarkable shift in the emission spectra on varying the solvent polarity. As shown in Fig. 4, the fluorescence peak is at 508 nm in toluene, the solvent of least polarity (0.36 D). In DMF, the solvent of highest polarity (3.82 D), the peak is located at 616 nm, which is red-shifted by 108 nm due to the changed molecular environment. Such behavior indicates significant charge redistribution upon excitation, which is also in agreement with the statement in the above Structural feature section. Besides, one can see that the fluorescence intensity of DBASVP in aprotic solvents decreases gradually with increasing solvent

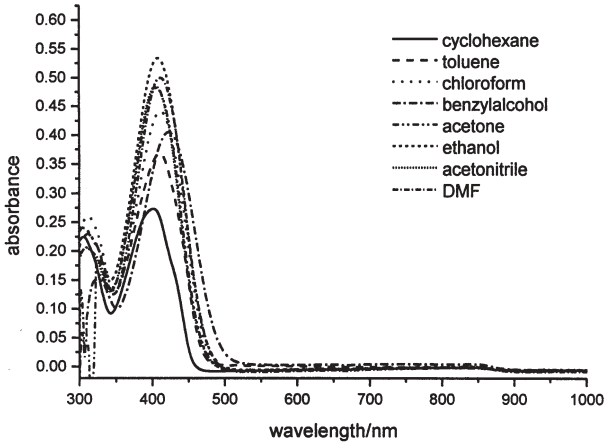

Fig. 3 Linear absorption spectra of DBASVP in solvents of different polarity at a concentration of 1×10^{-5} mol L^{-1}.

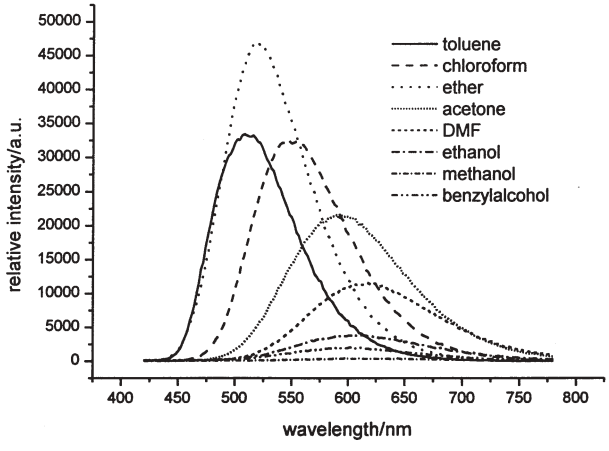

Fig. 4 Single-photon (of 450 W Xe arc lamp as excitation source) fluorescence spectra of DBASVP in different polarity solvents at a concentration of 1×10^{-5} mol L^{-1}.

Table 2 Stokes' shift ($\Delta\bar{\nu}$) of DBASVP in solvents with different orientational polarizability (Δf) (ε is the value at 25 °C unless specified otherwise)

Solvents	n	ε	$\lambda_{abs\text{-}max}$/ nm	$\lambda_{em\text{-}max}$/ nm	$\Delta\bar{\nu}$/ cm^{-1}	Δf
Cyclohexane	1.424	2.023[b]	402	488	4384	−0.0005
Toluene	1.494	2.379	408	508	4825	0.0140
Chloroform	1.444	4.806[b]	411	546	6016	0.1487
Diethyl ether	1.352	4.34[b]	398	518	5821	0.1672
Benzyl alcohol	1.538	13.1[b]	422	602	7085	0.2100
THF	1.404	7.58	405	550	6509	0.2107
DMF	1.427	37.6	411	616	8097	0.2760
Acetone	1.357	20.7	406	590	7681	0.2849
Ethanol	1.359	24.3	408	606	8008	0.2894
Acetonitrile	1.342	37.4	405	612	8351	0.3062

[a]The values of the refractive index (n) and relative permittivity are taken from ref. 23 . [b]Relative permittivities measured at 20 °C.

polarity except in ether, in which DBASVP exhibits the highest fluorescence intensity of all the solutions. In protic solvents, such as in ethanol, methanol and benzyl alcohol, DBASVP shows relatively low fluorescence intensity.

In order to further demonstrate the influence of solvent on fluorescence, Table 2 lists the Stokes' shift of DBASVP in solvents of different polarity. The Stokes' shift is defined as the loss of energy between absorption and reemission of light, which is a result of several dynamic processes. These processes include energy losses due to dissipation of vibrational energy, redistribution of electrons in the surrounding solvent molecules induced by the altered dipole moment of the excited chromophore, reorientation of the solvent molecules around the excited state dipole, and specific interactions between the fluorophore and the solvent or solutes. The Lippert equation is the most widely used equation to describe the effects of the physical properties of the solvent on the emission spectra of fluorophore.[16]

$$\bar{\nu}_a - \bar{\nu}_f \cong \frac{2}{hc}\left(\frac{\varepsilon-1}{2\varepsilon+1} - \frac{n^2-1}{2n^2+1}\right)\frac{(\mu_e - \mu_g)^2}{a^3} + const \quad (6)$$

In this equation, h is Planck's constant, c is the speed of light, and a is the radius of the cavity in which the fluorophore resides. The wavenumbers of the absorption and emission are $\bar{\nu}_a$ and $\bar{\nu}_f$ (in cm^{-1}). ε and n are the relative permittivity and the refractive index respectively. The terms in the first brackets are called the orientation polarizability (Δf). Fig. 5 shows a plot of $\bar{\nu}_a - \bar{\nu}_f$ *versus* the orientation polarizability. In aprotic solvents, Stokes' shifts are approximately proportional to the orientational polarizability. But no obvious shifts larger than expected are found in protic solvents, even though hydrogen bonds exist between the DBASVP molecules and the protic solvents. The specific solvent effect caused by protic solvents manifests itself in a decrease in fluorescence intensity (Fig. 4).

Based on eqn. (6) and Table 2, one can evaluate the charge separation of DBASVP upon excitation in aprotic solvents. Assuming that the cavity radius is 8.7 Å, which is comparable to the radius of DBASVP (the distance calculated between two nitrogen atoms is 17.4 Å), on the basis of eqn. (6), the difference in the calculated dipole moment between the ground and excited states in solution is 29.4 D, which is larger than that in a vacuum. It is known that a dipole moment of 4.8 D results from a charge separation of one unit charge (4.8×10^{-10} esu) by 1 Å. Hence, for DBASVP, 29.4 D corresponds to an intramolecular charge separation of 6.125 Å upon excitation. This fact indicates that DBASVP is highly dependent on solvent polarity. The redistribution of electrons occurs within the DBASVP molecule, which again proves that DBASVP possesses a highly delocalized conjugated system.

Fluorescence lifetime and quantum yield. The fluorescence lifetime measurement of DBASVP in solvents of different polarity was performed on the same Edinburgh FLS920 spectrofluorometer with a Hydrogen flash lamp (pulse duration <1 ns) as the excitation source. During the measurements, DBASVP was excited with the optimal excitation wavelength (λ_{max}^{ex}) in order to give the largest relative fluorescence intensity in each solution. Emission peaks were observed irrespective of the excitation wavelength. The time distribution of the hydrogen lamp pulse is measured immediately before the measurement of the fluorescence decay. The observed decay of fluorescence is given by convolution of the lamp pulse with the impulse response of the sample. The decays were analyzed by the "least-squares" and iterative reconvolution method. The quality of the exponential fits was evaluated by the goodness of fit (χ^2). For all the decays in this experiment, χ^2 is less than 1.2, which indicates a good fit. The results are shown in Fig. 6. The fluorescence lifetime of DBASVP in aprotic solvents increases with increases in solvent polarity. In protic solvents, DBASVP exhibits reduced lifetimes, especially in methanol, in which the value is less than 0.6 ns.

The photoluminescence quantum efficiencies in different solvents were measured on a Perkin Elmer LS-55B fluorospectrometer by comparison of the fluorescence intensities with that of compounds of known quantum yield under identical experimental conditions. The Rh6G ethanol solution was used as the quantum-yield standard ($\Phi = 0.97$), and a RhB ethanol

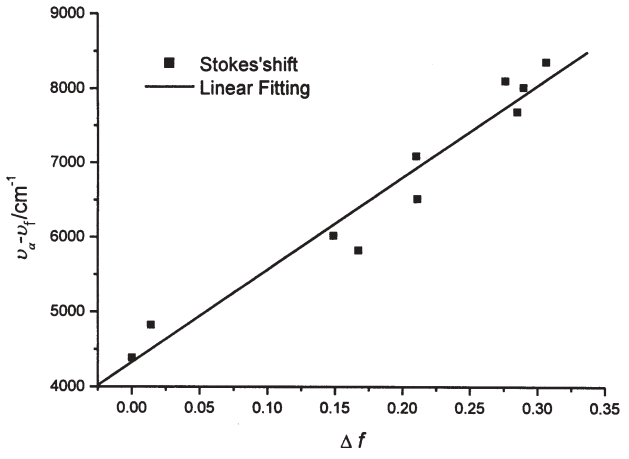

Fig. 5 Stokes' shift of DBASVP in various solvents *versus* orientation polarizability of the solvents. The concentration of solution measured was 1×10^{-5} mol L^{-1}.

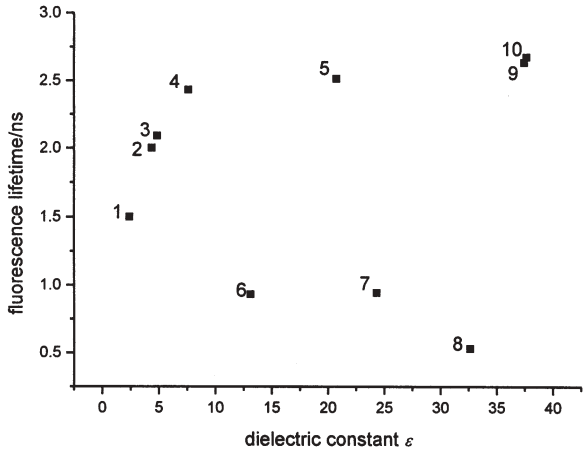

Fig. 6 Fluorescence lifetime of 1×10^{-5} mol L^{-1} DBASVP solutions in solvents of different polarity. 1 Toluene; 2 diethyl ether; 3 chloroform; 4 THF; 5 benzyl alcohol; 6 acetone; 7 ethanol; 8 methanol; 9 acetonitrile; 10 DMF.

Table 3 Fluorescence lifetime τ_f, quantum yield Φ_f, radiative rate constants $k_f = \Phi_f/\tau_f$ and nonradiative rate $k_{nr} = (1 - \Phi_f)/\tau_f$ of DBASVP in solvents of different polarity

Solvents	τ_f/ns	Φ_f	$k_f/10^7$ s^{-1}	$k_{nr}/10^7$ s^{-1}
Toluene	1.50	0.39	25.8	40.8
Benzyl alcohol	0.93	0.05	4.9	102.7
Methanol	0.59	0.06	10.3	159.2
DMF	2.67	0.04	1.5	35.9

solution was used to calibrate the system. 2×10^{-7} mol L^{-1} DBASVP dilute solutions were prepared in order to avoid possible aggregation and self-absorption. The quantum yield was calculated according to the following equation.[17]

$$\Phi_s = \Phi_r \left(\frac{A_r(\lambda_r)}{A_s(\lambda_s)}\right)\left(\frac{I(\lambda_r)}{I(\lambda_s)}\right)\left(\frac{n_s^2}{n_r^2}\right)\frac{\int F_s}{\int F_r} \quad (7)$$

Here, Φ is the quantum yield, n is the refractive index, $I(\lambda)$ is the relative intensity of the exciting light at wavelength λ, $A(\lambda)$ is the absorbance of the solution at the exciting wavelength λ, and $\int F$ is the integrated area under the corrected emission spectrum. Subscripts s and r refer to the sample and reference solutions, respectively. Radiative and nonradiative rate constants were also calculated and the results are listed in Table 3. One can see that the quantum yield and fluorescence lifetime of DBASVP in protic solvents are strongly reduced (the reduced fluorescence lifetime is also illustrated in Fig. 6). The very large nonradiative rates indicate the presence of an additional radiationless channel. We attribute the outstanding behavior of DBASVP in benzyl alcohol and methanol to the specific solvent effect of hydrogen bonding. Because the absorption spectrum remains unchanged in protic solvents (see Fig. 3), the ground-state complexation between DBASVP and protic solvents can be ruled out. Therefore, the formation of a nonfluorescent charge transfer excited state engaged in an excited hydrogen bonded pair is the very reason for the strongly reduced fluorescence yield.[18] Besides, the behavior of the DBASVP–DMF solution is noticeable. It possesses an equally small quantum yield as that shown by DBASVP in protic solution. Decreased quantum yields have frequently been reported for molecules with a similar structure to that of DBASVP in which the rotation of the C–N bond connecting the amino group to the chromophore forms a twisted intramolecular charge transfer (TICT) geometry.[19–21] According to the TICT model, the increase in polarity of the solvents will lower the energy level of the CT state, and thus the fluorescence emission peak will red shift. In addition, the TICT state will rapidly undergo nonradiative transition to triplets, and it results in a marked decrease in the fluorescence quantum yield with increasing solvent polarity. The red-shifted fluorescence peak shown in Fig. 4 and the markedly decreased fluorescence yield listed in Table 3 suggest that the TICT mechanism is also suitable for interpreting fluorescence behavior of the DBASVP–DMF solution.

4 Two-photon fluorescence

The experimental setup for two-photon fluorescence measurement is shown in Fig. 7. The laser beam from a mode-locked Ti:sapphire laser (Coherent Mira 900F) is the pump source with a pulse duration of 200 fs, a repetition rate of 76 MHz, and a single-scan streak camera (Hamamatsu Model C5680-01) together with a monochromator as the recorder. Using this experimental setup, the maximum two-photon fluorescence intensities at different excitation wavelengths were measured at identical pump energy levels of 0.380 W. The samples measured were 0.01 mol L^{-1} DBASVP–toluene and DBASVP–DMF solutions. A polarizer was used to keep the incident beam energy constant at different excited wavelength. The data

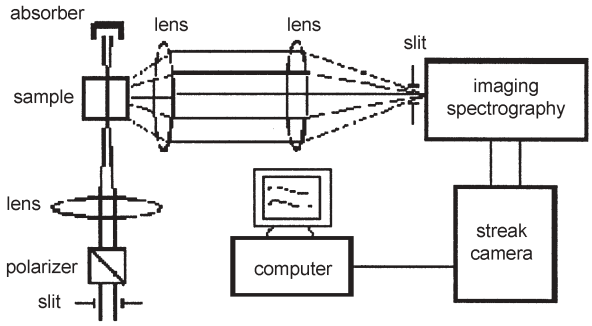

Fig. 7 Experimental setup for the measurement of the two-photon fluorescence intensity at different excitation wavelengths.

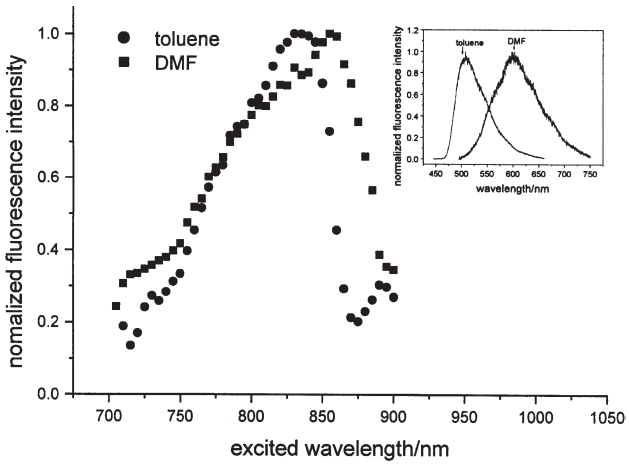

Fig. 8 Two-photon (from a 200 fs, 76 MHz Ti:sapphire laser) fluorescence intensity (peak) of DBASVP in toluene (circle) and DMF (square) *versus* excitation wavelengths of identical energy of 0.380 W. Insert: two-photon fluorescence spectra excited at 800 nm. The concentration of the solutions measured was 0.01 mol L^{-1}.

were recorded in the excitation wavelength range of 710 nm to 900 nm with a step size of 5 nm. The results are plotted in Fig. 8. Each datum expresses the maximum fluorescence intensity excited at each wavelength. One can see that the two-photon fluorescence intensity gradually increases with the red shift of the excited wavelength, and after a maximum, it decreases rapidly with the red shift of the excited wavelength. The maximum two-photon fluorescence emission was found to be excited by an 830 nm laser beam in toluene solution and an 855 nm laser beam in DMF solution, which indicates that the optimal absorption wavelengths of two-photon excitation for two DBASVP solutions are located at 830 nm and 855 nm respectively. Obviously, the two-photon absorption peak is red-shifted with increasing solvent polarity. The two-photon fluorescence spectra of DBASVP in these two solvents, excited at 800 nm, are also shown in Fig. 8 (inset). The fluorescence peaks at 508 nm in toluene, and is red-shifted to 600 nm in the more polar solvent of DMF. Therefore, for DBASVP, the solvatochromism of the two-photon process is similar to that of the single-photon process.

5 Two-photon photopolymerization

A grating was created by two-photon polymerization of a poly(urethane acrylate) oligomer using DBASVP as initiator. A film of the mixture of initiator and oligomer with a weight ratio of $\sim$2 to $\sim$3% (a little DMF solvent was added to control the viscosity) was prepared by spin-coating onto glass plates. The experimental setup is shown in Fig. 9. The same mode-locked Ti:sapphire laser as that used in the two-photon

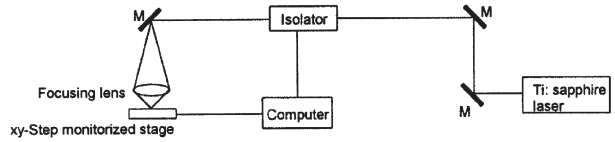

Fig. 9 Experimental setup for two-photon photopolymerization. M = mirror.

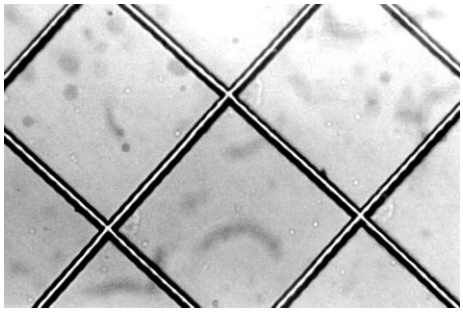

Fig. 10 Optical micrograph of the grating fabricated *via* two-photon polymerization of a poly(urethane acrylate) oligomer using DBASVP as initiator.

fluorescence measurements was used for two-photon microfabrication. It provided the 800 nm lasing source which was tightly focused *via* an objective lens ($\times 40$, NA = 0.65), and the focal point was focussed on the sample film on the xy-step monitorized stage controlled by computer. The pulse energy before being focused by the objective lens was ~ 1.2 W. The polymerized solid skeleton was obtained after any unreacted liquid mixture had been washed out. The grating fabricated was observed through a polarization microscope (Opton, Germany). Its photograph is illustrated in Fig. 10.

The photopolymerization mechanism of this new initiator is still unknown. According to Cumpston *et al*.,[22] strong donor substituents would make the conjugated system electron rich, and after one- or two-photon photoexcitation, these chromophores would be able to transfer an electron even to relatively weak acceptors, and that this process could be used to activate the polymerization reaction. DBASVP possesses strong donor and acceptor substituents, and its molecule is electron rich. As the two-photon absorption cross-section of DBASVP is large, the two-photon-induced electron transfer within the molecule should be efficient. DBASVP also has the virtue of excellent electron delocalizataion upon excitation, which is believed to be another necessary condition for it to easily initiate a two-photon photopolymerization reaction. The exact mechanism of photoinitiation is currently being investigated. The systematic study of the microstructure created by two-photon free-radical photopolymerization using DBASVP as the initiator will be reported in detail elsewhere.

Conclusion

A new two-photon photopolymerization initiator of DBASVP has been synthesized. Its two-photon absorption cross-section determined by quantum chemistry calculations is as high as 881.34×10^{-50} cm^4 s photon^{-1}. The experimental results showed that DBASVP is solvent-sensitive, which indicates there is significant charge redistribution upon excitation. A microstructure was fabricated by two-photon photopolymerization using this new initiator using the 800 nm irradiation of a Ti:sapphire femtosecond laser.

Acknowledgements

The authors would like to acknowledge Professor Chuan-Kui Wang for useful discussions on the theoretical calculations of a two-photon absorption cross-section. This work was supported by a grant for the State Key Program of China (G1998061402), partly supported by the National Natural Science Foundation of China (Grant No. 50173015) and the Scientific Research Foundation for Outstanding Young Scientists of Shandong Province of China (Grant No. 01BS24).

References

1 S. Kawata, H. Sun, T. Tanaka and K. Takada, *Nature*, 2001, **412**, 597–598.
2 H. Sun, V. Mizeikis, Y. Xu, S. Juodkazis, J. Ye, S. Matsuo and H. Misawa, *Appl. Phys. Lett.*, 2001, **79**, 1–3.
3 M. P. Joshi, H. E. Pudavar, J. Swiatkiewicz, P. N. Prasad and B. A. Reianhardt, *Appl. Phys. Lett.*, 1999, **74**, 170–172.
4 P. Galajda and P. Ormos, *Appl. Phys. Lett.*, 2001, **78**, 249–251.
5 S. M. Kuebler, B. H. Cumpson, S. Ananthavel, S. Barlow, J. E. Ehrlich, L. L. Etsine, A. A. Heikal, D. McCord-Maughon, J. Qin, H. Rocel, M. Rumi, S. R. Marder and J. W. Perry, *SPIE-Int. Soc. Opt. Eng.*, 2000, **3937**, 97–105.
6 M. Albota, D. Beljonne, J. L. Bredas, J. E. Ehrlich, J. Y. Fu, A. A. Heikal, S. E. Hess, T. Kogej, M. D. Levin, S. R. Marder, D. McCord-Maughon, J. W. Perry, H. Röckel, M. Rumi, G. Subramaniam, W. W. Webb, X. L. Wu and C. Xu, *Science*, 1998, **281**, 1653–1656.
7 B. A. Reinhardt, L. L. Brott, S. J. Clarson, A. G. Dillard, J. C. Bhatt, R. Kannan, L. X. Yuan, G. S. He and P. N. Prasad, *Chem. Mater.*, 1998, **10**, 1863–1874.
8 J. J. P. Stewart, *Quantum Chem. Program Exch.*, 1990, **10**, 86.
9 J. J. P. Stewart, *MOPAC 93.00 Manual*, Fujitsu Limited, Tokyo, 1993.
10 A. Klamt, *J. Phys. Chem.*, 1995, **99**, 2224–2235.
11 M. Karelson, K. Pihlaja and M. C. Zerner, *J. Photochem. Photobiol. A*, 1995, **85**, 119.
12 P. Macak, Y. Luo and H. Ågren, *J. Chem. Phys.*, 2001, **114**, 9813–9820.
13 Y. Luo, P. Macak, P. Norman, C. K. Wang and H. Ågren, *Nonlinear Opt.*, 2001, **27**, 33–46.
14 P. Fromherz, *J. Phys. Chem.*, 1995, **99**, 7188–7192.
15 U. Narang, C. F. Zhao, J. D. Bhawalkar, F. V. Bright and P. N. Prasad, *J. Phys. Chem.*, 1996, **100**, 4521–4525.
16 J. R. Lakowicz, *Principles of Fluorescence Spectroscopy*, Plenum Press, New York, 1983, p. 190.
17 J. N. Demas and G. A. Crosby, *J. Phys. Chem.*, 1971, **75**, 991–1024.
18 M. Maus, W. Rettig, D. Bonafoux and R. Lapouyade, *J. Phys. Chem. A*, 1999, **103**, 3388–3401.
19 J. D. Simon and S. G. Su, *J Chem. Phys.*, 1987, **87**, 7016–7023.
20 R. K. Guo, N. Kitamura and S. Tazuke, *J. Phys. Chem.*, 1990, **94**, 1404–1408.
21 G. S. He, L. Yuan, Y. Cui, M. Li and P. N. Prasad, *J. Appl. Phys.*, 1997, **81**, 2529–2537.
22 B. H. Cumpston, S. P. Ananthavel, S. Barlow, D. L. Dyer, J. E. Ehrlich, L. L. Erskine, A. A. Heikal, S. M. Kuebler, I.-Y. Sandy Lee, D. McCord-Maughon, J. Qin, H. Röckel, M. Rumi, X. L. Wu, S. R. Marder and J. W. Perry, *Nature*, 1999, **398**, 51–54.
23 *CRC Handbook of Chemistry and Physics*, ed. D. R. Lide, CRC Press, Boca Raton, FL, 73rd edn., 1992–1993.